Radiation pattern of a classical dipole in a photonic crystal: Photon focusing

Dmitry N. Chigrin*
Institute of Materials Science and Department of Electrical and Information Engineering, University of Wuppertal, Gauss-strasse 20, 42097 Wuppertal, Germany

(Received 25 June 2003; revised manuscript received 2 August 2004; published 18 November 2004)

An asymptotic analysis of the radiation pattern of a classical dipole in a photonic crystal possessing an incomplete photonic bandgap is presented. The far-field radiation pattern demonstrates a strong modification with respect to the dipole radiation pattern in vacuum. Radiated power is suppressed in the direction of the spatial stop band and strongly enhanced in the direction of the group velocity, which is stationary with respect to a small variation of the wave vector. An effect of radiated power enhancement is explained in terms of *photon focusing*. A numerical example is given for a square-lattice two-dimensional photonic crystal. Predictions of asymptotic analysis are substantiated with finite-difference time-domain calculations, revealing a reasonable agreement.

DOI: 10.1103/PhysRevE.70.056611 PACS number(s): 42.70.Qs, 42.25.Fx, 42.50.Pq, 81.05.Zx

I. INTRODUCTION

Purcell [1] was the first who pointed out that the spontaneous emission of an atom or a molecule depends on its environment. Since then, the influence of nontrivial boundary conditions in the vicinity of an excited atom on its emissive properties has been the subject of active research [2–4]. Important examples of such an influence are an enhancement and inhibition of the spontaneous emission by a resonant environment [1] —e.g., microcavity. These phenomena were first demonstrated by Goy *et al.* [5] and Kleppner [6], respectively, and continue to be the subject of intense research not only due to their contribution to the better understanding of the light matter interaction, but to a great extent, due to the practical importance of controlling the light emission process. Light-emitting diodes [7–9] and thresholdless lasers [10–12] are just a few examples, where the light extraction and the spontaneous emission control by means of optical microcavity lead to improved performance.

The dielectric periodic medium, also called photonic crystal [13,14], is a good example of nontrivial boundary conditions on an electromagnetic field. Such an inhomogeneous medium can possess a complete photonic band gap—i.e., a continuous spectral range within which linear propagation of light is prohibited in all spatial directions. One of the consequences is an inhibited spontaneous emission for the atomic transition frequency inside the complete photonic band gap [15–17]. There are no electromagnetic modes avaliable to carry the energy away from the atom at complete photonic band gap frequencies. Although the existence of a complete photonic band gap usually requires dielectric materials with relatively high refractive index ($n>2$) arranged in a three-dimensional (3D) lattice [13,14], photonic crystals are proved to be useful artificial materials to modify the light emission even in the absence of complete photonic band gap. For example, it was demonstrated that the external quantum efficiency of light-emitting diodes can be significantly improved by introducing a two-dimensional (2D) photonic crystal [18,19]. Another example is a highly directive light source employing a 3D photonic crystal [20,21].

An intrinsic property of photonic crystals is their complicated photonic band structure, which can be engineered by choosing an appropriate combination of materials and lattice geometry [13,14]. Being able to modify in purpose the emission rate within a specific spectral range and simultaneously in specific directions could add a significant flexibility in improving light sources.

A number of papers were devoted to the study of the spontaneous emission in photonic crystals [15–17,22–32]. But to the author's knowledge, questions like the modification of the emission rate in a specific direction and modification of the emission pattern due to the photonic crystal environment have not been yet addressed. Special opportunities in controlling the directionality of emission exist within the spectral ranges of allowed photonic bands, where photonic crystals display strong dispersion and anisotropy. The consequence of anisotropy is the beam-steering effect [33,34], which in essence means that the group velocity direction of the medium's eigenmode does not necessarily coincide with its wave vector direction. A beam-steering effect is known to be the reason for a number of anomalies in an electromagnetic beam propagation inside a photonic crystal, which are usually referred to as superprism or ultrarefractive phenomena [33–35]. For example, an extraordinary large or negative beam bending [35], beam self-collimation [36,37], and photon focusing [38,39] were reported. The last phenomenon is similar to phonon focusing, a phenomenon observed in the ballistic transport of phonons in crystalline solids [40].

The term "phonon focusing" refers to the strong anisotropy of heat flux in crystalline solids. First observed in 1969 by Taylor *et al.* [41], phonon focusing is a property of all crystals at low temperatures. The term "focusing" does not imply a bending of particle paths, as in the geometrical-optics sense of the term. The physical reason for the phonon focusing is the beam steering. In particular, waves with quite

*Present address: Physikalisches Institut, Universität Bonn, Nussallee 12, 53115 Bonn, Germany.
Electronic address: chigrin@th.physik.uni-bonn.de

different wave vectors can have nearly the same group velocity, so the energy flux associated with those waves bunches along certain crystalline directions. In some special cases, a heat flux can display intricate focusing caustics, along which flux tends to infinity [40]. This happens when the direction of the group velocity is stationary with respect to a small variation of the wave vector.

One can expect that a similar phenomenon takes place in photonic crystals [38,39]. An optical cousin of the acoustic phenomenon opens a unique opportunity to design a caustics pattern on purpose, enhancing and suppressing emission in specific directions.

In this paper a description of the angular distribution of the radiated power of a classical dipole embedded in a photonic crystal is presented. It is assumed that only propagating modes of the photonic crystal contribute to the far-field radiation. The emission process is treated using an entirely classical model, similar to the one in [22,24]. Then in the steady-state limit the spontaneous emission rate Γ is related to the classical radiated power $P(\mathbf{r}_0)=(\omega/2)\mathrm{Im}[\mathbf{d}^*\cdot E(\mathbf{r}_0)]$ via $\Gamma=P/\hbar\omega$ [42], where $\mathbf{d}$ is a real dipole moment, $\mathbf{E}(\mathbf{r}_0)$ is a field in the system, and $\mathbf{r}_0$ is the dipole location.

The general expressions for the field and emission rate of the point dipole radiating in an arbitrary periodic medium are reviewed in Sec. II. The evaluation of the asymptotic form of the radiated field is given in Sec. III. In Sec. IV, the angular distribution of the radiated power is introduced. A modification of the radiation pattern is discussed in terms of photon focusing in Sec. V. A numerical example of an angular distribution of emission power radiated from the point isotropic light source is presented in Sec. VI for the case of a two-dimensional square lattice photonic crystal of dielectric rods in air. Summary is given in Sec. VII.

II. NORMAL-MODE EXPANSION OF DIPOLE FIELD

In this paper, a general linear, nonmagnetic, dielectric medium with arbitrary 3D periodic dielectric function $\varepsilon(\mathbf{r})=\varepsilon(\mathbf{r}+\mathbf{R})$ is studied. Here $\mathbf{R}$ is a vector of the direct Bravais lattice, $\mathbf{R}=\Sigma_i\, l_i\mathbf{a}_i$, l_i is an integer, and $\mathbf{a}_i$ is a basis vector of the periodic lattice. It is assumed that a medium is infinitely extended in space and that no absorption happens. To treat the emission process the mode radiation theory [43] is used in the framework of the classical electrodynamics [14,22,24]. In this section, the main results reported in [22,24] are reviewed.

In Gaussian units, Maxwell's equations in such a medium have the form

$$\nabla\times\mathbf{E}=-\frac{1}{c}\frac{\partial\mathbf{H}}{\partial t}, \tag{1}$$

$$\nabla\times\mathbf{H}=\frac{1}{c}\varepsilon(\mathbf{r})\frac{\partial\mathbf{E}}{\partial t}+\frac{4\pi}{c}\mathbf{J}, \tag{2}$$

$$\nabla\cdot[\varepsilon(\mathbf{r})\mathbf{E}]=0, \tag{3}$$

$$\nabla\cdot\mathbf{H}=0. \tag{4}$$

Here, the electric (magnetic) field is denoted by $\mathbf{E}$ ($\mathbf{H}$), and c is a speed of light in vacuum. An electromagnetic field is produced by a current source $\mathbf{J}$ and the charge density is zero, $\rho\equiv 0$. Then one can choose the transverse (Coulomb) gauge for the vector potential $\mathbf{A}$ in the form [43]

$$\nabla\cdot[\varepsilon(\mathbf{r})\mathbf{A}]=0. \tag{5}$$

The absence of the charge density implies that the scalar potential φ is zero. The electric and magnetic fields can be written in terms of the vector potential $\mathbf{A}$ via

$$\mathbf{E}=-\frac{1}{c}\frac{\partial\mathbf{A}}{\partial t}, \tag{6}$$

$$\mathbf{H}=\nabla\times\mathbf{A}. \tag{7}$$

Combining Eqs. (6) and (7) with Maxwell's equations (1)–(4) one obtains the wave equation for the vector potential $\mathbf{A}$:

$$\nabla\times\nabla\times\mathbf{A}+\frac{1}{c^2}\varepsilon(\mathbf{r})\frac{\partial^2\mathbf{A}}{\partial t^2}=\frac{4\pi}{c}\mathbf{J}. \tag{8}$$

In what follows, a simplest form of the current density $\mathbf{J}$ is taken,

$$\mathbf{J}(\mathbf{r},t)=-i\omega_0\mathbf{d}\,\delta(\mathbf{r}-\mathbf{r}_0)e^{-i\omega_0 t}, \tag{9}$$

for a harmonically oscillating dipole with a frequency ω_0 and a real dipole moment $\mathbf{d}$, located at the position $\mathbf{r}_0$ inside a photonic crystal, switched on at $t=0$.

The field of an arbitrary light source embedded in a periodic medium can be constructed by a suitable superposition of the medium's eigenwaves (e.g., [44]):

$$\mathbf{A}(\mathbf{r},t)=\sum_n\int_{BZ}d^3\mathbf{k}_n C_{n\mathbf{k}}(t)\mathbf{A}_{n\mathbf{k}}(\mathbf{r}). \tag{10}$$

Here $\mathbf{A}_{n\mathbf{k}}(\mathbf{r})$ and $C_{n\mathbf{k}}(t)$ are the Bloch eigenvector (normal modes) and the time-dependent amplitude coefficient of the eigenwave $(n,\mathbf{k})$, respectively. The form of the amplitude coefficient is defined by the particular nature of the light source. The integration is performed over the first Brillouin zone (BZ) of the crystal and the summation is carried out over different photonic bands, where n is the band index and $\mathbf{k}$ is the wave vector.

Eigenwaves $\mathbf{A}_{n\mathbf{k}}(\mathbf{r})$ satisfy the homogeneous wave equation

$$\nabla\times\nabla\times\mathbf{A}_{n\mathbf{k}}-\frac{\omega_{n\mathbf{k}}^2}{c^2}\varepsilon(\mathbf{r})\mathbf{A}_{n\mathbf{k}}=\mathbf{0} \tag{11}$$

and also fulfill the orthogonalization, normalization, and closure conditions given by

$$\int_V d^3\mathbf{r}\,\varepsilon(\mathbf{r})\mathbf{A}_{n\mathbf{k}}(\mathbf{r})\mathbf{A}^*_{n'\mathbf{k}'}(\mathbf{r})=V\delta_{nn'}\delta(\mathbf{k}-\mathbf{k}'), \tag{12}$$

$$\int d^3\mathbf{k} \mathrm{A}_{n\mathbf{k}}(\mathbf{r})\mathbf{A}^*_{n\mathbf{k}}(\mathbf{r}') = \mathcal{I}_{\varepsilon_\perp}\delta(\mathbf{r}-\mathbf{r}'), \tag{13}$$

where $\omega_{n\mathbf{k}}$ is the Bloch eigenfrequency, V is the volume of the unit cell of the crystal, * denotes the complex conjugate, and $\mathcal{I}_{\varepsilon_\perp}$ is the identity operator on the subset of the ε-transverse vector functions as defined in [43]. The Bloch eigenvector $\mathbf{A}_{n\mathbf{k}}(\mathbf{r})$ obeys the gauge condition $\boldsymbol{\nabla}\cdot[\varepsilon(\mathbf{r})\mathbf{A}_{n\mathbf{k}}(\mathbf{r})]=0$ and is therefore transverse with respect to this gauge. Equations (12) and (13) ensure that the eigenvectors $\mathbf{A}_{n\mathbf{k}}(\mathbf{r})$ form a complete set of orthonormal ε-transverse functions. Here any vector that satisfies the ε-transverse gauge condition (5) is called "ε-transverse" [22].

The amplitude coefficients $C_{n\mathbf{k}}(t)$ can be easily obtained from the wave equation (8). Then, the electromagnetic field at the point $\mathbf{r}$ radiated by the point dipole located at $\mathbf{r}_0$ can be represented in terms of Bloch modes as

$$\mathbf{A}(\mathbf{r},t) = -i\frac{4\pi c\omega_0}{V}\sum_n \int_{BZ} d^3\mathbf{k}_n \frac{[\mathbf{a}^*_{n\mathbf{k}}(\mathbf{r}_0)\cdot\mathbf{d}]}{(\omega^2_{n\mathbf{k}}-\omega^2_0)} \times \mathrm{a}_{n\mathbf{k}}(\mathbf{r})e^{i\mathbf{k}_n\cdot(\mathbf{r}-\mathbf{r}_0)}e^{-i\omega_0 t}, \tag{14}$$

where the Bloch theorem $\mathbf{A}_{n\mathbf{k}}(\mathbf{r})=\mathbf{a}_{n\mathbf{k}}(\mathbf{r})e^{i\mathbf{k}_n\cdot\mathbf{r}}$ has been used.

The integrand in Eq. (14) has a pole at $\omega^2_{n\mathbf{k}}=\omega^2_0$, and the integral is singular. This is a typical behavior for any resonance system, where dissipation is neglected. The standard way to regularize the integral is to add a small imaginary part to ω^2_0. The result of the integration then becomes dependent on the sign of this imaginary part. The criterion for determining the sign will be discussed below. A regularized integral (14) reads

$$\mathbf{A}(\mathbf{r},t) = -i\frac{4\pi c\omega_0}{V}\sum_n \int_{BZ} d^3\mathbf{k}_n \frac{[\mathbf{a}^*_{n\mathbf{k}}(\mathbf{r}_0)\cdot\mathbf{d}]}{(\omega^2_{n\mathbf{k}}-\omega^2_0-i\gamma)} \times \mathbf{a}_{n\mathbf{k}}(\mathbf{r})e^{i\mathbf{k}_n\cdot(\mathbf{r}-\mathbf{r}_0)}e^{-i\omega_0 t}. \tag{15}$$

When a light source is situated in an inhomogeneous medium, it is immersed in its own electric field emitted at an earlier time and reflected from inhomogeneities in the medium (radiation reaction field). By conservation of energy, the decay rate at which energy is radiated is equal to the rate at which the charge distribution of the source does work on the surrounding electromagnetic field. For an arbitrary current density $\mathbf{J}$, the radiated power is given by [45]

$$P(t) = -\int_V d^3\mathbf{r}\mathbf{J}(\mathbf{r},t)\cdot\mathbf{E}(\mathbf{r},t), \tag{16}$$

where V is a volume containing a current density source $\mathbf{J}$ and it is related to spontaneous emission rate via $\Gamma=P/\hbar\omega_0$ [42]. Then, the time-averaged radiated power of the point dipole (9) is given by

$$P = \frac{\omega_0}{2}\mathrm{Im}[\mathbf{d}^*\cdot\mathbf{E}(\mathbf{r}_0)], \tag{17}$$

which can be interpreted as the emission rate modification due to the dipole interaction with the out-of-phase part of the radiation reaction field [46,47].

To define the radiation reaction field, let us consider an excited molecule or atom at a position $\mathbf{r}_0$ in a photonic crystal. Assuming that the presence of the molecule does not change the band structure of the crystal, the only possible mode it can emit in is an eigenmode of the photonic crystal. Then, the radiation reaction field can be chosen in the form of the normal mode expansion (15), which is valid for any point $\mathbf{r}$ in the crystal, which is distinct from (but as close as required to) the dipole location $\mathbf{r}_0$. Then the radiated power (emission rate) (17) of the classical dipole in a photonic crystal is given by [22,24]

$$P = \frac{\pi^2\omega_0^2}{V}\sum_n \int d^2\mathbf{k}_n \frac{|\mathbf{A}_{n\mathbf{k}}(\mathbf{r}_0)\cdot\mathbf{d}|^2}{|\mathbf{V}_{n\mathbf{k}}|}, \tag{18}$$

where $\mathbf{V}_{n\mathbf{k}}=\boldsymbol{\nabla}_{\mathbf{k}}\omega_{n\mathbf{k}}$, the group velocity of the eigenwave $(n,\mathbf{k})$ is introduced.

Formula (18) gives the total time-averaged radiated power of the dipole situated inside a photonic crystal in the instantaneous backaction regime. It reflects the possible emission rate modification due to photonic crystal environment in the steady-state limit, while keeping emission dynamics modification out of the consideration. The internal dynamics of the emitter (emission, absorption, reemission, reabsorption, etc.) is completely lost within this approximation by the specific choice of the test dipole (9) (the radiation reaction field). This approximation corresponds to the Weisskopf-Wigner approximation in the quantum theory of the spontaneous emission of a two-level atom in an inhomogeneous medium [30,43]. Although the chosen approximation gives the correct result for emission rate modification in most of the situations considered in the presented paper, special care should be taken for frequencies near the photonic band edges or other van Hove singularities, where the instantaneous backaction approximation is broken due to a significant modification of emission dynamics [17,30].

III. ASYMPTOTIC FORM OF DIPOLE FIELD

In this section, a radiating dipole field is analyzed in the radiation zone. For that, an asymptotic form of the integral (15) is evaluated and analyzed. In what follows, an asymptotic analysis of the Green's function developed by Maradudin [48] for the phonon scattering problem is used.

Using the integral representation

$$\frac{1}{x-i\gamma} = -\frac{1}{i}\int_0^\infty d\tau e^{-ix\tau-\gamma\tau}, \tag{19}$$

one can rewrite Eq. (15) as

$$\mathbf{A}(\mathbf{r}) = \frac{4\pi c\omega_0}{V}\sum_n \int_{BZ} d^3\mathbf{k}_n \times \int_0^\infty d\tau[\mathbf{a}^*_{n\mathbf{k}}(\mathbf{r}_0)\cdot\mathbf{d}]\mathbf{a}_{n\mathbf{k}}(\mathbf{r})e^{iF_{n\mathbf{k}}(\tau)}, \tag{20}$$

where

$$F_{n\mathbf{k}}(\tau) = \mathbf{k}_n\cdot(\mathbf{r}-\mathbf{r}_0) - \tau(\omega^2_{n\mathbf{k}}-\omega^2_0) \tag{21}$$

and a limit $\gamma\to 0$ was taken.

In a typical experiment $|\mathbf{x}|=|\mathbf{r}-\mathbf{r}_0|\gg\lambda$, where λ is the wavelength of the electromagnetic wave. For large $|\mathbf{x}|$ an exponential function in the integral (20) will oscillate very rapidly and one can use the method of stationary phase to evaluate the integral.

The principal contribution to the integral comes from the neighborhood of those points in τ and $\mathbf{k}$ space where the variation of $F_{n\mathbf{k}}(\tau)$ is the smallest. This means that one can set the gradient of the function $F_{n\mathbf{k}}(\tau)$ in $\mathbf{k}$ space equal to zero as well as the derivative of the function with respect to τ. This gives the conditions

$$\frac{\partial F_{n\mathbf{k}}}{\partial \tau} = \omega_{n\mathbf{k}}^2 - \omega_0^2 = \mathbf{0}, \tag{22}$$

$$\boldsymbol{\nabla}_{\mathbf{k}} F_{n\mathbf{k}} = \mathbf{x} - \tau \boldsymbol{\nabla}_{\mathbf{k}} \omega_{n\mathbf{k}}^2 = 0. \tag{23}$$

Equations (22) and (23) determine the values of τ and $\mathbf{k}_n$ around which the principal contributions to the integral (20) arise. These points are called stationary points. Further, the stationary points are denoted by τ_ν and $\mathbf{k}_n^\nu$. Assuming that value of the eigenvector $\mathbf{a}_{n\mathbf{k}}(\mathbf{r})$ is approximately constant $\mathbf{a}_{n\mathbf{k}}(\mathbf{r}) \approx \mathbf{a}_{n\mathbf{k}}^\nu(\mathbf{r})$ for τ close to τ_ν and for the wave vectors close to $\mathbf{k}_n^\nu$, the integral (20) is reduced to the sum of the integrals in the vicinities of the stationary points $(\tau_\nu, \mathbf{k}_n^\nu)$ [48,49]:

$$\mathbf{A}(\mathbf{r}) \approx \frac{4\pi c\omega_0}{V} \sum_n \sum_\nu [\mathbf{a}_{n\mathbf{k}}^{\nu *}(\mathbf{r}_0)\cdot\mathbf{d}]\mathbf{a}_{n\mathbf{k}}^\nu(\mathbf{r}) \times \int_{\mathbf{k}_n^\nu} d^3\mathbf{k}_n \int_{\tau_\nu} d\tau e^{iF_{n\mathbf{k}}(\tau)}. \tag{24}$$

Here an extra summation is over all possible solutions of Eqs. (22) and (23).

Due to Eq. (22), the principal contribution to the asymptotic behavior of $\mathbf{A}(\mathbf{r})$ comes from the isofrequency surface in $\mathbf{k}$ space defined by $\omega_{n\mathbf{k}}^2 = \omega_0^2$ or equivalently defined by $\omega_{n\mathbf{k}} = \omega_0$ (eigenfrequency $\omega_{n\mathbf{k}}$ is positive and real). At the same time, due to Eq. (23) , the portion of the isofrequency surface $\omega_{n\mathbf{k}} = \omega_0$, which contributes to the asymptotic field, is the portion near the point on this surface where the gradient $\boldsymbol{\nabla}_{\mathbf{k}}\omega_{n\mathbf{k}}^2$ is parallel to $\mathbf{x}$. One can express the latter condition in an alternative fashion. Equation (23) can be simplified as

$$\mathbf{x} = 2\tau\omega_{n\mathbf{k}}\mathbf{V}_{n\mathbf{k}},$$

where $\mathbf{V}_{n\mathbf{k}} = \boldsymbol{\nabla}_{\mathbf{k}}\omega_{n\mathbf{k}}$ is the group velocity of the eigenwave $(n,\mathbf{k})$. So Eq. (23) just says that the principal contribution to the asymptotic behavior of the field $\mathbf{A}(\mathbf{r})$ at large $|\mathbf{x}|=|\mathbf{r}-\mathbf{r}_0| \gg \lambda$ comes from the neighborhood of the points $\mathbf{k}_n^\nu$ on the isofrequency surface $\omega_{n\mathbf{k}} = \omega_0$ at which the eigenwave group velocity is collinear to observation direction $\mathbf{x}$. Since τ is positive by definition (19), $\mathbf{V}_{n\mathbf{k}}^\nu$ and $\mathbf{x}$ should not only be collinear, but should point in the same direction as well—i.e., $\mathbf{x}\cdot\mathbf{V}_{n\mathbf{k}}^\nu > 0$.

Assuming that the major contribution comes from the regions near the stationary points, one makes a little error by extending the integration in Eq. (24) over all space:

$$\mathbf{A}(\mathbf{r}) \approx \frac{4\pi c\omega_0}{V} \sum_n \sum_\nu [\mathbf{a}_{n\mathbf{k}}^{\nu *}(\mathbf{r}_0)\cdot\mathbf{d}]\mathbf{a}_{n\mathbf{k}}^\nu(\mathbf{r}) \times \int_{-\infty}^{\infty} d^3\mathbf{k}_n \int_{-\infty}^{\infty} d\tau e^{iF_{n\mathbf{k}}(\tau)}. \tag{25}$$

Then, the integral over τ is simply given by a Dirac δ function,

$$\int_{-\infty}^{\infty} d\tau e^{i\tau(\omega_0^2 - \omega_{n\mathbf{k}}^2)} = 2\pi\delta(\omega_0^2 - \omega_{n\mathbf{k}}^2),$$

and one can further convert the volume integration in $\mathbf{k}$ space to an integral over the isofrequency surface $\omega_{n\mathbf{k}} = \omega_0$. In fact, by using the relations $|\boldsymbol{\nabla}_{\mathbf{k}}\omega_{n\mathbf{k}}|dk = d\omega_{n\mathbf{k}}$ and $d^3\mathbf{k} = dkd^2\mathbf{k}$, and integrating over the eigenfrequency $\omega_{n\mathbf{k}}$, the volume integration over $\mathbf{k}$ transforms to

$$\int_{-\infty}^{\infty} d^3\mathbf{k}_n e^{i\mathbf{k}_n(\mathbf{r}-\mathbf{r}_0)}\delta(\omega_0^2 - \omega_{n\mathbf{k}}^2) = \oint_{-\infty}^{\infty} d^2\mathbf{k}_n \frac{\pi}{\omega_0}\frac{e^{i\mathbf{k}_n\cdot(\mathbf{r}-\mathbf{r}_0)}}{|\mathbf{V}_{n\mathbf{k}}|},$$

where $\mathbf{V}_{n\mathbf{k}} = \nabla_{\mathbf{k}}\omega_{n\mathbf{k}}$ is the group velocity of the eigenwave $(n,\mathbf{k})$. So the asymptotic form of the field $\mathbf{A}(\mathbf{r})$ is given finally by

$$\mathbf{A}(\mathbf{r}) \approx \frac{4\pi^2 c}{V} \sum_n \sum_\nu \frac{[\mathbf{a}_{n\mathbf{k}}^{\nu *}(\mathbf{r}_0)\cdot\mathbf{d}]\mathbf{a}_{n\mathbf{k}}^\nu(\mathbf{r})}{|\mathbf{V}_{n\mathbf{k}}^\nu|} \oint_{-\infty}^{\infty} d^2\mathbf{k}_n e^{i\mathbf{k}_n\cdot(\mathbf{r}-\mathbf{r}_0)}, \tag{26}$$

where the comparatively slowly varying function $\mathbf{V}_{n\mathbf{k}}$ was replaced by its value at stationary point $\mathbf{k}_n^\nu$ and was taken outside the integral over $\mathbf{k}$.

To evaluate the integrals in Eq. (26) the analysis of the form of the isofrequency surface in the vicinity of one of the stationary points, $\mathbf{k}_n^\nu$, should be done. It is convenient to introduce the local curvilinear coordinates ξ_i with the origin at the stationary point and with one of the coordinates aligned perpendicular to the isofrequency surface—e.g., ξ_3. One can expand function $h(\xi_1,\xi_2) = \mathbf{k}_n\cdot\hat{\mathbf{x}}$ near the stationary point as

$$h(\xi_1,\xi_2) = \mathbf{k}_n^\nu\cdot\hat{\mathbf{x}} + \frac{1}{2}\sum_{i,j=1}^{2}\alpha_{ij}^\nu\xi_i\xi_j + \frac{1}{6}\sum_{i,j,k=1}^{2}\beta_{ijk}^\nu\xi_i\xi_j\xi_k + O(\xi_1,\xi_2)^4, \tag{27}$$

where

$$\alpha_{ij}^\nu = \left(\frac{\partial^2 h}{\partial\xi_i\partial\xi_j}\right)_\nu, \quad \beta_{ijk}^\nu = \left(\frac{\partial^3 h}{\partial\xi_i\partial\xi_j\partial\xi_k}\right)_\nu,$$

and $\hat{\mathbf{x}}$ is a unit vector in the observation direction. All derivatives are evaluated at the stationary point $\mathbf{k}_n^\nu$.

The result of the integration in Eq. (26) depends on the local topology of the isofrequency surface near the stationary point. One can generally classify the local topology of the surface by its Gaussian curvature. The Gaussian curvature K is the product of the two principal curvatures (inverse radii, K_1 and K_2) at a point on the surface—i.e., $K = K_1K_2$. The points on an isofrequency surface can be elliptical, hyperbolic, and parabolic. If the Gaussian curvature $K>0$, the corresponding point on the isofrequency surface is called el-

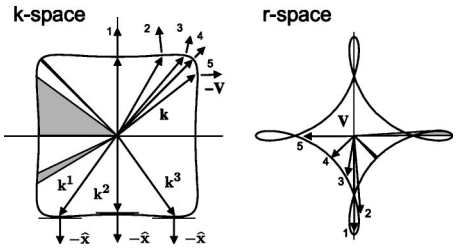

FIG. 1. Isofrequency and wave contours. Left: the central region of the isofrequency contour for normalized frequency $\Omega=\omega d/2\pi c=d/\lambda=0.569$ of an infinite square-lattice 2D photonic crystal made out of dielectric rods placed in vacuum. Rods have the refractive index 2.9 and radius $r=0.15d$, where d is the period of the lattice (see Sec. VI for details). The stationary points $\mathbf{k}^1$, $\mathbf{k}^2$, and $\mathbf{k}^3$, corresponding to the same observation direction $\hat{\mathbf{x}}$ are indicated. Right: corresponding wave contour with folds. The shaded and black regions show how two equal solid-angle sections in coordinate space (right) map to widely varying solid-angle sections in $\mathbf{k}$ space (left). The wave and group velocity vectors with numbers illustrate the fold formation of the wave contour.

liptical, and if $K<0$, it is called hyperbolic. For a complex surface, such as the isofrequency surface in Fig. 1, left, the regions with positive and negative Gaussian curvature alternate. The surface is parabolic at the borders between regions with curvatures of opposite signs—e.g, convex and saddle. The lines along which the curvature changes its sign are called parabolic lines. The Gaussian curvature at a parabolic point is equal to zero.

Further, the analysis of the asymptotic form of the integral (26) is undertaken, when the stationary points are elliptical or hyperbolic. Then in the close vicinity of such a stationary point the following expansion holds:

$$h(\xi_1,\xi_2)=\mathbf{k}_n^\nu\cdot\hat{\mathbf{x}}+\frac{1}{2}\sum_{i,j=1}^{2}\alpha_{ij}^\nu\xi_i\xi_j, \tag{28}$$

where only quadratic terms in the expansion (27) were kept. By choosing the orientation of the local coordinates ξ_1 and ξ_2 along the main directions of the surface curvature at that point $\mathbf{k}_n=\mathbf{k}_n^\nu$, one can diagonalize the matrix α_{ij}^ν. Then,

$$h(\xi_1,\xi_2)=\mathbf{k}_n^\nu\cdot\hat{\mathbf{x}}+\frac{1}{2}(\alpha_1^\nu\xi_1^2+\alpha_2^\nu\xi_2^2),\quad \alpha_1^\nu=\alpha_{11}^\nu,\ \alpha_2^\nu=\alpha_{22}^\nu. \tag{29}$$

With such a choice of local coordinates in $\mathbf{k}$ space, the product $K_{n\mathbf{k}}^\nu=\alpha_1^\nu\alpha_2^\nu$ determines the Gaussian curvature of the isofrequency surface at the stationary point $\mathbf{k}_n=\mathbf{k}_n^\nu$.

Using expansion (29) the asymptotic form of the field (26) is now given by

$$\mathbf{A}(\mathbf{r})\approx\frac{4\pi^2c}{V}\sum_n\sum_\nu\frac{[\mathbf{a}_{n\mathbf{k}}^{\nu*}(\mathbf{r}_0)\cdot\mathbf{d}]\mathbf{a}_{n\mathbf{k}}^\nu(\mathbf{r})}{|\mathbf{V}_{n\mathbf{k}}^\nu|}e^{i\mathbf{k}_n^\nu\cdot\mathbf{x}}\times\oint_{-\infty}^{\infty}d\xi_1d\xi_2\exp\left(\frac{i|\mathbf{x}|}{2}(\alpha_1^\nu\xi_1^2+\alpha_2^\nu\xi_2^2)\right). \tag{30}$$

The integral in Eq. (30) is calculated simply to be

$$\int_{-\infty}^{\infty}d\xi\,\exp\left(i\frac{x\alpha}{2}\xi^2\right)=\sqrt{\frac{2\pi}{x|\alpha|}}\exp\left(-\frac{i\pi}{4}\mathrm{sgn}(\alpha)\right), \tag{31}$$

and an asymptotic form of the vector potential (14) at the position $\mathbf{r}$ far from the dipole is given by

$$\mathbf{A}(\mathbf{r},t)\approx\sum_n\sum_\nu\exp\left[-i\left(\omega_0t+\frac{\pi}{4}[\mathrm{sgn}(\alpha_1^\nu)+\mathrm{sgn}(\alpha_2^\nu)]\right)\right]\times\frac{c}{V}\frac{[\mathbf{A}_{n\mathbf{k}}^{\nu*}(\mathbf{r}_0)\cdot\mathbf{d}]\mathbf{A}_{n\mathbf{k}}^\nu(\mathbf{r})}{|\mathbf{V}_{n\mathbf{k}}^\nu|}\frac{8\pi^3}{|K_{n\mathbf{k}}^\nu|^{1/2}|\mathbf{r}-\mathbf{r}_0|}, \tag{32}$$

where $\mathbf{A}_{n\mathbf{k}}^\nu(\mathbf{r})=\mathbf{a}_{n\mathbf{k}}^\nu(\mathbf{r})e^{i\mathbf{k}_n^\nu\cdot\mathbf{r}}$ and summation is over all stationary points with $\mathbf{x}\cdot\mathbf{V}_{n\mathbf{k}}^\nu>0$.

According to Eq. (32) the electromagnetic field inside the photonic crystal represents a superposition of several diverging waves, the number of which equals the number of stationary phase points on the isofrequency surface $\omega_{n\mathbf{k}}=\omega_0$ (Fig. 1, left). Each of these waves has its own shape and its own propagation velocity. One comment is important here: the asymptotic expansion (32) describes an outgoing wave ($\mathbf{k}_n^\nu\cdot\mathbf{x}>0$) only if the corresponding group velocity is an outward normal to the isofrequency surface $\omega_{n\mathbf{k}}=\omega_0$ at point $\mathbf{k}_n^\nu$. It can happen, however, that the group velocity becomes an inward normal for some frequencies and regions of $\mathbf{k}$ space (Fig. 1, left). In such a case the dot product $\mathbf{k}_n^\nu\cdot\mathbf{x}$ is not positive in the asymptotic expansion (32) and the expansion describes incoming waves. In such a situation, one should change the sign of the small imaginary part γ in regularized equation (15) [48],

$$\mathbf{A}(\mathbf{r})=-i\frac{4\pi c\omega_0}{V}\sum_n\int_{BZ}d^3\mathbf{k}_n\frac{[\mathbf{a}_{n\mathbf{k}}^*(\mathbf{r}_0)\cdot\mathbf{d}]}{(\omega_{n\mathbf{k}}^2-\omega_0^2+i\gamma)}\times\mathbf{a}_{n\mathbf{k}}(\mathbf{r})e^{i\mathbf{k}_n\cdot(\mathbf{r}-\mathbf{r}_0)}, \tag{33}$$

and proceed as has been described above, Eqs. (20)–(32), but using the integral representation

$$\frac{1}{x+i\gamma}=\frac{1}{i}\int_0^\infty d\tau e^{ix\tau-\gamma\tau} \tag{34}$$

instead of Eq. (19).

IV. ANGULAR DISTRIBUTION OF RADIATED POWER

In this section, the angular dependence of the dipole radiated power (18) is introduced.

Using the definition of the solid angle, $d\Omega_{n\mathbf{k}}=d^2\mathbf{k}\cos\varphi/|\mathbf{k}_n|^2$, where $d\Omega_{n\mathbf{k}}$ is the solid angle subtended by the surface element $d^2\mathbf{k}_n$, φ is the angle between the wave vector $\mathbf{k}_n$, and the group velocity $\mathbf{V}_{n\mathbf{k}}=\nabla_{\mathbf{k}}\omega_{n\mathbf{k}}$ (Fig. 2), on changing the integration variables, one can modify Eq. (18) to the form

$$P=\sum_n\int_0^{4\pi}d\Omega_{n\mathbf{k}}\left(\frac{\pi^2\omega_0^2}{V}\frac{|\mathbf{A}_{n\mathbf{k}}(\mathbf{r}_0)\cdot\mathbf{d}|^2}{|\mathbf{V}_{n\mathbf{k}}|}\frac{|\mathbf{k}_n|^2}{\cos\varphi}\right), \tag{35}$$

where the function enclosed in the brackets defines the radiated power of the dipole per solid angle in $\mathbf{k}$ space:

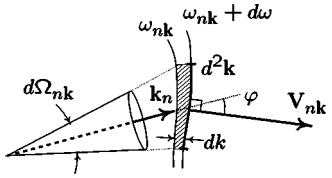

FIG. 2. Diagram showing the relations between **k** space and coordinate space quantities. Isofrequency contours for frequencies $\omega_{n\mathbf{k}}$ and $\omega_{n\mathbf{k}}+d\omega$ are presented.

$$\frac{dP}{d\Omega_{n\mathbf{k}}}=\frac{\pi^2\omega_0^2}{V}\frac{|\mathbf{A}_{n\mathbf{k}}(\mathbf{r}_0)\cdot\mathbf{d}|^2}{|\mathbf{V}_{n\mathbf{k}}|}\frac{|\mathbf{k}_n|^2}{\cos\varphi}. \tag{36}$$

To derive the angular distribution of radiated power in coordinate space, one should change the integration variables in Eq. (35) from **k** space to coordinate space (Fig. 3).

The **k**-space distribution of the radiated power (36) is a function of the **k**-space direction, given by the polar, $\theta_{n\mathbf{k}}$, and azimuthal, $\phi_{n\mathbf{k}}$, angles of the wave vector $\mathbf{k}_n$. The direction of energy propagation in a nonabsorbing periodic medium coincides with the group velocity direction [50], whereas the coordinate-space angular dependence of the radiated power is given by the corresponding group velocity direction in coordinate space (θ,ϕ). Here θ and ϕ are the polar and azimuthal angles of the group velocity in coordinate space. The **k** space to coordinate space transformation may be expressed formally as

$$\cos\theta=f(\cos\theta_{n\mathbf{k}},\phi_{n\mathbf{k}}), \tag{37}$$

$$\phi=g(\cos\theta_{n\mathbf{k}},\phi_{n\mathbf{k}}), \tag{38}$$

where the functions f and g are determined from the components of the group velocity vector $\mathbf{V}_{n\mathbf{k}}^{\nu}\|\hat{\mathbf{x}}$, where $\hat{\mathbf{x}}$ is a unit vector in the observation direction. The Jacobian of the transformation, Eqs. (37) and (38),

$$J_{n\mathbf{k}}=\frac{\partial f}{\partial\cos\theta_{n\mathbf{k}}}\frac{\partial g}{\partial\phi_{n\mathbf{k}}}-\frac{\partial f}{\partial\phi_{n\mathbf{k}}}\frac{\partial g}{\partial\cos\theta_{n\mathbf{k}}}, \tag{39}$$

relates a small solid angle in coordinate space with the corresponding solid angle in **k** space via

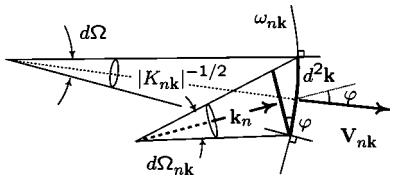

FIG. 3. Diagram to derive the relation between solid angles in **k** space and coordinate space. The isofrequency contour for frequency $\omega_{n\mathbf{k}}$ is presented. The Jacobian of the transformation, Eqs. (37) and (38), is given by the ratio $d\Omega/d\Omega_{n\mathbf{k}}$. By the definition of the solid angle, the solid angle in **k** space is $d\Omega_{n\mathbf{k}}=d^2\mathbf{k}\cos\varphi/|\mathbf{k}_n|^2$, while the corresponding solid angle in coordinate space is $d\Omega=d^2\mathbf{k}|K_{n\mathbf{k}}|$. That gives the Jacobian $J_{n\mathbf{k}}=|\mathbf{k}_n|^2|K_{n\mathbf{k}}|/\cos\varphi$. Here φ is an angle between the wave vector and the group velocity vector. $d^2\mathbf{k}$ is the surface element of the isofrequency surface.

$$d\Omega=d(\cos\theta)d\phi=J_{n\mathbf{k}}d(\cos\theta_{n\mathbf{k}})d\phi_{n\mathbf{k}}=J_{n\mathbf{k}}d\Omega_{n\mathbf{k}}. \tag{40}$$

According to the results presented in Sec. III, different wave vectors can result in the group velocity with same direction in coordinate space. That means that the equation

$$d\Omega_{n\mathbf{k}}^{\nu}=\frac{1}{J_{n\mathbf{k}}^{\nu}}d\Omega$$

should hold for each stationary wave vector, which satisfies $\hat{\mathbf{x}}\cdot\mathbf{V}_{n\mathbf{k}}^{\nu}>0$. Changing the integration variables in Eq. (35) one should then sum individual contributions from all these wave vectors:

$$P=\sum_n\sum_{\nu}\int_0^{4\pi}d\Omega\left(\frac{\pi^2\omega_0^2}{V}\frac{|\mathbf{A}^{\nu}{}_{n\mathbf{k}}(\mathbf{r}_0)\cdot\mathbf{d}|^2}{J_{n\mathbf{k}}^{\nu}|\mathbf{V}_{n\mathbf{k}}^{\nu}|}\frac{|\mathbf{k}_n^{\nu}|^2}{\cos\varphi}\right). \tag{41}$$

The geometrical relationship between solid angles in **k** space and coordinate space (Fig. 3) results in the following formula for the Jacobian (39):

$$J_{n\mathbf{k}}^{\nu}=|\mathbf{k}_n^{\nu}|^2|K_{n\mathbf{k}}^{\nu}|/\cos\varphi.$$

Then, Eq. (41) can be transformed to the form

$$P=\int_0^{4\pi}d\Omega\left(\sum_n\sum_{\nu}\frac{\pi^2\omega_0^2}{V}\frac{|\mathbf{A}_{n\mathbf{k}}^{\nu}(\mathbf{r}_0)\cdot\mathbf{d}|^2}{|\mathbf{V}_{n\mathbf{k}}^{\nu}||K_{n\mathbf{k}}^{\nu}|}\right), \tag{42}$$

where $\mathbf{V}_{n\mathbf{k}}^{\nu}=\boldsymbol{\nabla}_{\mathbf{k}}\omega_{n\mathbf{k}}$ is the group velocity and $K_{n\mathbf{k}}^{\nu}$ determines the Gaussian curvature of the isofrequency surface at the stationary point $\mathbf{k}_n=\mathbf{k}_n^{\nu}$. Finally, the radiated power of the dipole per solid angle in coordinate space is given by the function enclosed in the brackets in Eq. (42):

$$\frac{dP}{d\Omega}=\sum_n\sum_{\nu}\frac{\pi^2\omega_0^2}{V}\frac{|\mathbf{A}_{n\mathbf{k}}^{\nu}(\mathbf{r}_0)\cdot\mathbf{d}|^2}{|\mathbf{V}_{n\mathbf{k}}^{\nu}||K_{n\mathbf{k}}^{\nu}|}. \tag{43}$$

Formula (43) provides a simple route to calculate an angular distribution of radiated power of the point dipole (9) inside a photonic crystal. It can be interpreted as a decay rate at which the dipole transfers energy to the electromagnetic waves with the group velocity in the observation direction. Then, $(d\Gamma/d\Omega)=(dP/d\Omega)/\hbar\omega_0$ is related to the probability of the radiative transition of an excited atom with emitting a photon traveling in the given observation direction.

Basically, formulas (42) and (43) involve calculations of the Bloch wave vectors $\mathbf{k}_n^{\nu}$, ending at the isofrequency surface $\omega_{n\mathbf{k}}=\omega_0$, the corresponding group velocity vectors $\mathbf{V}_{n\mathbf{k}}^{\nu}$, the Gaussian curvature of the isofrequency surface $K_{n\mathbf{k}}^{\nu}$, and the local coupling strength of the dipole moment with a Bloch eigenwave $(n,\mathbf{k})$, given by the factor $|\mathbf{A}_{n\mathbf{k}}^{\nu}(\mathbf{r}_0)\cdot\mathbf{d}|$. The primary difficulty in obtaining the coordinate-space distribution of radiated power $(dP/d\Omega)$, Eq. (43), is that the wave vector, the group velocity, and the Gaussian curvature are all functions of the **k**-space direction, whereas the angular dependence of the radiative power $(dP/d\Omega)$ is given by the corresponding group velocity direction (θ,ϕ). To calculate the radiated power $(dP/d\Omega)$, Eq. (43), one should take an inverse of the mapping, Eqs. (37) and (38). This inverse is not necessarily unique. In the case of multiple stationary points (22) and (23), one direction (θ,ϕ) results from several different **k**-space directions $(\theta_{\mathbf{k}},\phi_{\mathbf{k}})$ (Fig. 1). This requires

that the inversion of the mapping, Eqs. (37) and (38), must be done point by point.

As a simple exercise, formula (43) is applied here to calculate an angular distribution of power radiated by a dipole in free space. The wave vector and the group velocity in free space are parallel and their values are simply given by $|\mathbf{k}| = \omega_0/c$ and c, respectively. The Gaussian curvature of the isofrequency surface is a square of the inverse wave vector $1/|\mathbf{k}|^2$. And the appropriate normal modes are plane waves,

$$\mathbf{A}_{n\mathbf{k}}(\mathbf{r}) = \sqrt{\frac{V}{(2\pi)^3}} e^{i\mathbf{k}\cdot\mathbf{r}} \hat{\mathbf{a}}_{n\mathbf{k}},$$

where $\hat{\mathbf{a}}_{n\mathbf{k}}$ is a polarization vector orthogonal to the wave vector $\mathbf{k}$. Then, the radiated power is given by Eq. (43),

$$\left(\frac{dP}{d\Omega}\right)_{free} = \frac{1}{8\pi}\frac{\omega_0^4}{c^3}|\mathbf{d}|^2 \sin^2\theta, \tag{44}$$

yielding the usual results for radiation pattern in free space [45].

V. PHOTON FOCUSING

The factor $|\mathbf{A}^{\nu}_{n\mathbf{k}}(\mathbf{r}_0)\cdot\mathbf{d}|^2$ in relation (43), giving the coupling strength of dipole moment with the photonic crystal eigenmode at the dipole position, can display a complex angular behavior, which depends on the eigenmode structure and dipole orientation with respect to the crystal lattice. To study the net result of the influence of a photonic crystal on the radiation pattern of the emitter, it is instructive to model an isotropic light source producing a uniform distribution of wave vectors. Moreover, an isotropic point source is usually a good model for a common experimental situation of emitters with random distribution of dipole moment (dye molecules [51–55], quantum dots [51,56], etc.). Then, the radiated power (43) should be averaged over the dipole moment orientation, which simply yields a factor of $|\mathbf{d}|^2/3$:

$$\left(\frac{dP}{d\Omega}\right)_i = \sum_n \sum_\nu \frac{(2\pi c)^3}{V\omega_0^2} \frac{|\mathbf{A}^{\nu}_{n\mathbf{k}}(\mathbf{r}_0)|^2}{|\mathbf{V}^{\nu}_{n\mathbf{k}}||K^{\nu}_{n\mathbf{k}}|}. \tag{45}$$

Here the result was normalized to the radiated power in free space. Now, the factor $|\mathbf{A}^{\nu}_{n\mathbf{k}}(\mathbf{r}_0)|^2$ gives the field strength at the source position and has no angular dependence. So the radiation pattern of a point isotropic emitter is defined by

$$\left(\frac{dP}{d\Omega}\right)_i \sim \sum_n \sum_\nu |\mathbf{V}^{\nu}_{n\mathbf{k}}|^{-1}|K^{\nu}_{n\mathbf{k}}|^{-1}. \tag{46}$$

The radiated power (46) is proportional to the inverse group velocity $|\mathbf{V}^{\nu}_{n\mathbf{k}}|^{-1}$ and to the inverse Gaussian curvature $|K^{\nu}_{n\mathbf{k}}|^{-1}$ of the isofrequency surface. A large enhancement of the emission rate is expected when the group velocity is small. This can be interpreted as a consequence of the long interaction time of the emitter and the radiation field [57–59]. In a similar fashion, a small Gaussian curvature formally implies an enhancement of the radiated power along a certain observation direction. While spontaneous emission enhancement due to a small group velocity involves a nonlinear interaction of the radiation and emitter, the enhancement due to a small Gaussian curvature is a linear phenomenon related to the anisotropy of the photonic crystal and is a result of the beam-steering effect. Being a measure of the rate with which emitter transfers energy in photons with a given group velocity, the radiated power (46) will be enhanced if many photons with different wave vectors reach the same detector. The enhancement of the radiated power, which is due to the small Gaussian curvature, is called *photon focusing* [38,39] and has a major influence on the radiation pattern of the point source in a photonic crystal.

The physical picture of *photon focusing* can be illustrated in the following manner (Fig. 1). An isofrequency surface of an isotropic and homogeneous medium is a sphere. There is only one stationary point with $\hat{\mathbf{x}}\cdot\mathbf{V}^{\nu}_{n\mathbf{k}} > 0$ and thus only one wave propagating in the given direction. Figure 1, left, is an example of a part of the actual isofrequency contour of a 2D photonic crystal made out of dielectric rods placed in vacuum (see Sec. VI for further details). The anisotropy of the crystal implies a complex nonspherical isofrequency surface, which can have several stationary points with $\hat{\mathbf{x}}\cdot\mathbf{V}^{\nu}_{n\mathbf{k}} > 0$ (Fig. 1, left). Several waves can propagate in a given direction inside a photonic crystal. It is illustrative to construct the *wave surface* in coordinate space. To construct the wave surface one should plot a ray in the observation direction $\hat{\mathbf{x}}$ starting from the point source position and having the length of the group velocity $|\mathbf{V}^{\nu}_{n\mathbf{k}}|$. An example of the wave contour is presented in Fig. 1, right. The existence of multiple stationary points implies that the wave surface is a complex multivalued surface parametrized by wave vector $\mathbf{k}_n$. Figure 1 illustrates how this can result in a fold of the wave surface.

In the vicinity of the parabolic point with zero Gaussian curvature an isofrequency surface is flat. That implies that a very large number of eigenwaves with wave vectors in the vicinity of a parabolic point have nearly the same group velocity, contributing to the energy flux in the direction parallel to that group velocity. In Fig. 1, it is illustrated by mapping two equal solid-angle sections along different observation directions in coordinate space onto the corresponding solid-angle sections in $\mathbf{k}$ space [60]. The black solid-angle section in coordinate space maps onto a single smaller solid-angle section in $\mathbf{k}$ space, implying a "defocusing" of the energy flux. The shaded solid-angle section in coordinate space, which crosses three different branches of the wave contour, maps onto two different and larger solid-angle sections in $\mathbf{k}$ space, implying enhancement ("focusing") of the energy flux in this group velocity direction. This results in a strongly varying angular distribution of the emission intensity with sharp singularities (caustics).

VI. NUMERICAL EXAMPLE: 2D PHOTONIC CRYSTAL

In this section the theoretical approach developed in the previous sections is applied to the numerical calculation of the radiation pattern of a point source placed inside a 2D photonic crystal. A point source is situated inside the crystal and it produces an isotropic and uniform distribution of wave vectors $\mathbf{k}_n$ with the frequency ω_0.

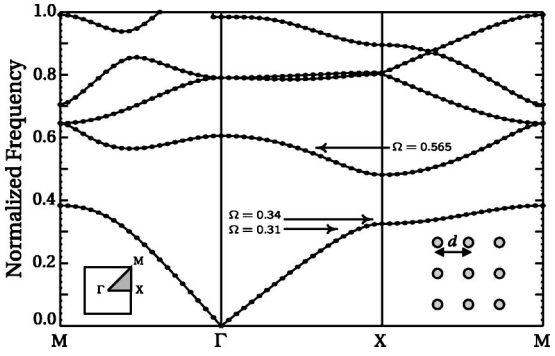

FIG. 4. Photonic band structure of TM modes for the square-lattice photonic crystal with refractive index of the rods $n=2.9$, lattice constant d, and radius of the rods $0.15d$. The frequency is normalized to $\Omega=\omega d/2\pi c=d/\lambda$. Here c is the speed of light in vacuum. The insets show the first Brillouin zone of the crystal with the irreducible zone shaded light gray (left) and a part of the lattice (right).

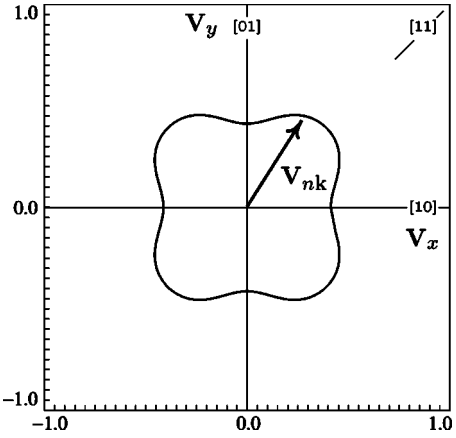

FIG. 6. Wave contour corresponding to the normalized frequency $\Omega=0.31$.The group velocity is plotted in units of the speed of light in vacuum. High-symmetry directions of the square lattice are specified.

An infinite 2D square lattice of dielectric rods in vacuum (Fig. 4) is considered in the case of in-plane propagation. Consequently, the problem of an electromagnetic wave interaction with a 2D photonic crystal is reduced to two independent problems, which are called TE and TM, when the magnetic or electric field is parallel to the axis of the rods. In the illustrative example presented in this section, all numerical calculations have been performed for TM modes of the crystal. The photonic band structure of the crystal made of the rods with the refractive index $n=2.9$ is presented in Fig. 4. The band structure has been calculated using the plane wave expansion method [61].

In Fig. 5 isofrequency contours of the crystal are presented for two frequencies belonging to the first photonic band (Fig. 4). To plot an isofrequency contour, the photonic band structure for all wave vectors within the irreducible BZ was calculated and then the equation $\omega(\mathbf{k})=\omega_0$ was solved for a given frequency ω_0. Frequencies have been chosen below ($\Omega=0.31$) and above ($\Omega=0.34$) the low edge frequency of the stop band in the ΓX direction of the crystal. The isofrequency contours below and above the stop band edge frequency show an important difference. As the frequency stays below the stop band, the isofrequency contour is *closed* and almost circular (Fig. 5). The corresponding wave contour (see Sec. V for definition) is presented in Fig. 6. To calculate the group velocity, the plane-wave expansion method [61] and the Hellmann-Feynman [14] theorem were used. The group velocity $|\mathbf{V}^{\nu}_{n\mathbf{k}}|$ and the Gaussian curvature $|K^{\nu}_{n\mathbf{k}}|$ of the isofrequency contours are relatively slow functions of the wave vector. The Gaussian curvature does not vanish for any wave vector. This implies a small anisotropy in the energy flux inside the crystal.

To find how a radiated power varies in coordinate space, one should calculate the group velocity and the Gaussian curvature on the isofrequency contour $\omega(\mathbf{k})=\omega_0$ as functions of the angle in coordinate space. As the wave contour is a single-valued function, the inverse of the mapping, Eqs. (37) and (38), from $\mathbf{k}$ space to coordinate space is one to one and can be easily done. In Fig. 7 a polar plot of the radiated power is presented, which shows a small amount of anisotropy.

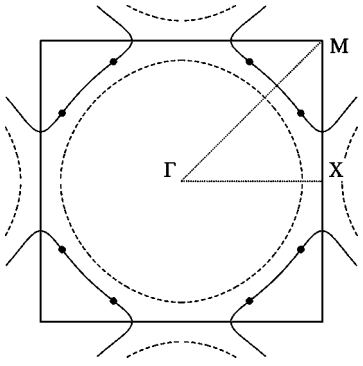

FIG. 5. Isofrequency contours of the square-lattice photonic crystal for the normalized frequencies $\Omega=0.31$ (dashed line) and $\Omega=0.34$ (solid line). The parabolic points are marked by the black dots. The first Brillouin zone of the lattice is plotted in order to show the spatial relation between zone boundary and isofrequency contours.

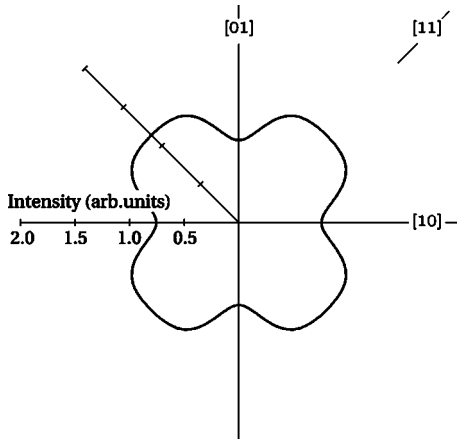

FIG. 7. Angular distribution of radiated power corresponding to the normalized frequency $\Omega=0.31$. High-symmetry directions of the square lattice are specified.

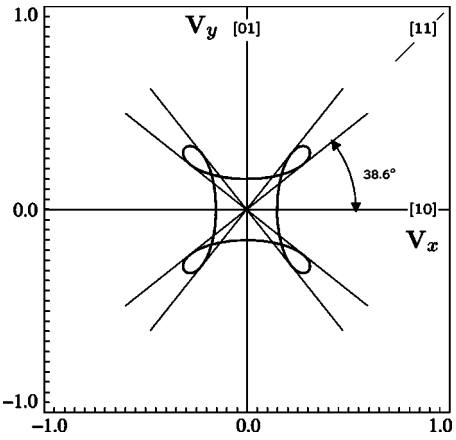

FIG. 8. Wave contour corresponding to the normalized frequency $\Omega=0.34$. The group velocity is plotted in units of the speed of light in vacuum. The directions corresponding to the folds of the wave contour are shown.

tropy. The angular distribution of the radiated power possesses fourfold rotational symmetry of the crystal.

With an increase of the frequency up to the stop band, the topology of the isofrequency contour abruptly changes. The stop band developes in the ΓX direction and the isofrequency contour becomes *open* (Fig. 5). This topology changes the result in the complex contour with alternating regions of different Gaussian curvature signs. Parabolic points, where the Gaussian curvature vanishes, are marked by black dots in Fig. 5. As has been discussed in Sec. V, a vanishing curvature results in the folds of the wave contour. The wave contour corresponding to the isofrequency $\Omega=0.34$ is presented in Fig. 8. A pair of the parabolic points in the first quarter of the Brillouin zone results in a cuspidal structure of the wave contours in the first quarter of coordinate space. This dramatically increases anisotropy of the energy flux.

The folds in the wave contours yield that the inverse of the mapping, Eqs. (37) and (38), from **k** space to coordinate space is not one to one anymore. To apply the formula (46)

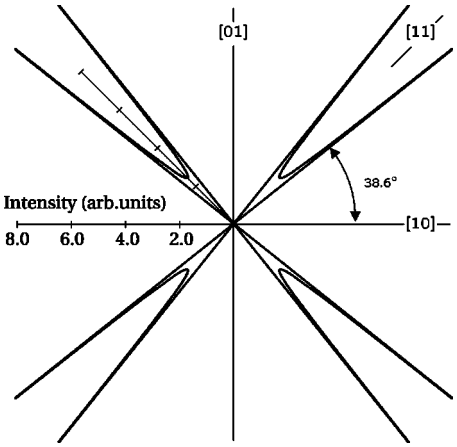

FIG. 9. Angular distribution of the radiated power corresponding to the normalized frequency $\Omega=0.34$. The directions of infinite radiated power (caustic) coincide with the directions of the folds of the wave contour (Fig. 8).

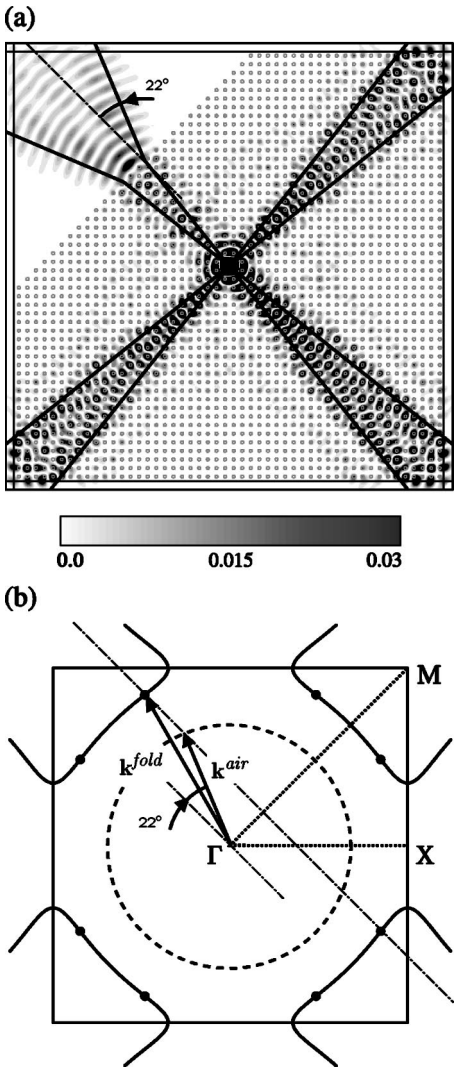

FIG. 10. (a) FDTD calculation. Map of the modulus of the Poynting vector field for a 50×50 rods photonic crystal excited by a point isotropic source with the normalized frequency $\Omega=0.34$. The location of the crystal in the simulation domain is shown together with asymptotic directions of photon focusing caustics. (b) Isofrequency contours of the square lattice photonic crystal (solid line) and air (dashed line) for normalized frequency $\Omega=0.34$. The dash-dotted line is a construction line. The wave vector corresponding to the parabolic point (black dot), $\mathbf{k}^{fold}$, and the wave vector in air, obtained from the momentum conservation law at the crystal–air interface, $\mathbf{k}^{air}$, are shown.

to calculate the angular distribution of the radiated power in such a case, one should proceed as follows. At first, the Gaussian curvature as a function of the wave vector should be calculated. Then, wave vectors and group velocities corresponding to the parabolic points on the isofrequency surface should be found. An inversion of the mapping, Eqs. (37) and (38), should be calculated separately for each of the branches of the wave contour. The total radiated power is a sum of the different contributions from these branches. In Fig. 9 the polar plot of the radiated power (46) corresponding to the normalized frequency $\Omega=0.34$ is presented. The energy flux is strongly anisotropic for this frequency, showing a

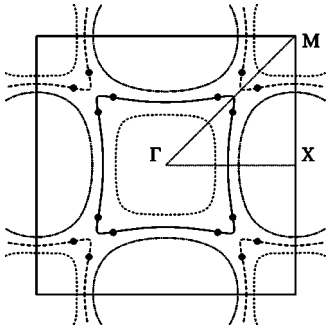

FIG. 11. Isofrequency contours of the square-lattice photonic crystal for the normalized frequencies $\Omega=0.55$ (dotted line), $\Omega=0.565$ (solid and dashed lines) and $\Omega=0.58$ (dash-dotted line). Two branches of the isofrequency contour of $\Omega=0.565$ are plotted as solid and dashed lines. The parabolic points are marked by the black dots. The first Brillouin zone of the lattice is plotted in order to show the spatial relation between the zone boundary and isofrequency contours.

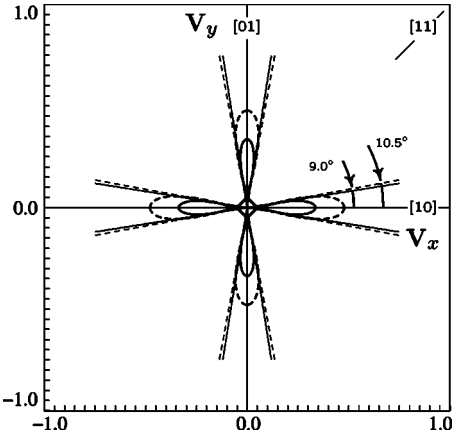

FIG. 12. Wave contours corresponding to the normalized frequency $\Omega=0.565$. Solid (dashed) wave contour corresponds to solid (dashed) isofrequency contour in Fig. 11. The group velocity is plotted in the units of the speed of light in vacuum. The directions corresponding to the folds of the wave contour are shown.

relatively small intensity in the directions of the stop band and infinite intensity (caustics) in the directions of the folds.

To substantiate this behavior, finite-difference time domain (FDTD) calculations were done [62,63]. The simulated structure was a 50×50 lattice of dielectric rods in vacuum [Fig. 10(a)]. The top-left corner of the lattice was removed, allowing the radiation to leave the structure and to refract at the crystal–air interface. The simulation domain was discretized into squares with a side $\Delta=d/16$. The total simulation region was 800×800 cells plus a 16-cell-wide perfectly matched layer (PML) [64]. The point isotropic light source was modeled by a current density source [62,63] with a homogeneous spacial dependence and sinusoidal temporal dependence of the signal. FDTD calculations were performed using the code described in Ref. [65].

In Fig. 10(a) a map of the modulus of the Poynting vector field is shown. The point source is placed in the middle of the crystal. The field map is shown for one instant time step. The snapshots were captured after 4096 time steps, where the time step was 0.99 of the Courant value. The structure of the crystal is superimposed on the field map. From Fig. 10(a) one can see that the emitted light is focused in the directions coinciding with the predicted directions of the folds (black lines inside the crystal).

The radiation experiences refraction when it approaches the photonic crystal–air interface [Fig. 10(a)]. To predict the focusing direction outside the crystal the wave vector diagram can be analyzed [Fig. 10(b)]. In Fig. 10(b), isofrequency contours of the crystal (solid line) and air (dashed line) for normalized frequency $\Omega=0.34$ together with the construction line (dash-dotted line) are shown. The construction line is a line, which is perpendicular to the crystal–air interface. Applying the momentum conservation law to the tangential component of the wave vector at the parabolic point, the wave vector of refracted wave can be obtained. One can see from Fig. 10(b) that such a simple analysis gives a reasonable agreement with the rigorous FDTD calculations.

In Figs. 11–13, a more complicated example of the anisotropy of a photonic crystal is presented. Isofrequency contours for three frequencies belonging to the second photonic band of the crystal are plotted in Fig. 11. While isofrequency contours for the normalized frequencies $\Omega=0.55$ and $\Omega=0.58$ have nonvanishing Gaussian curvature for all wave vectors leading to only a limited anisotropy of the energy flux, the isofrequency contour for the normalized frequencies $\Omega=0.565$ displays several parabolic points. Moreover, the isofrequency contour consists of two branches with slightly different shapes (solid and dashed lines in Fig. 11). Two branches yield two wave contours with cuspidal folds in coordinate space (Fig. 12). Applying the formula (46) to the radiated power calculation, one should sum over contributions coming from all branches of the wave contours in coordinate space. An angular distribution of radiated power for the normalized frequencies $\Omega=0.565$ is presented in Fig. 13. Within the first quarter of coordinate space, four caustics with infinite radiated power present in the energy flux corre-

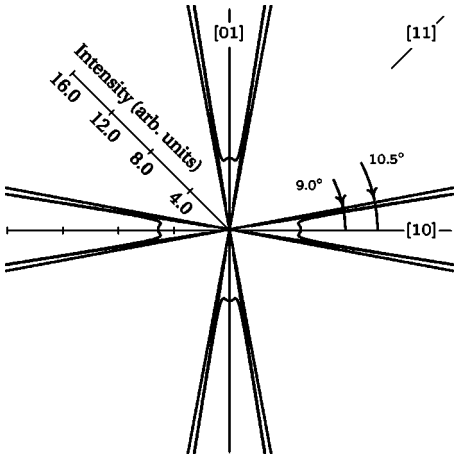

FIG. 13. Angular distribution of radiated power corresponding to the normalized frequency $\Omega=0.565$. The directions of infinite radiative power (caustic) coincide with the directions of the folds of the wave contour.

sponded to four parabolic points on two branches of the isofrequency contours.

VII. SUMMARY

In this paper, by analyzing a dipole field in the radiation zone it was shown that the principal contribution to the far field of the dipole radiating in a photonic crystal comes from the regions of the isofrequency surface in the wave vector space at which the eigenwave group velocity is parallel to observation direction $\hat{\mathbf{x}}$. It was also shown that the anisotropy of a photonic crystal reveals itself in the strongly nonspherical wave front, leading to modifications of both the far-field radiation pattern and spontaneous emission rate. By systematic analysis of the Maxwell equations a simple formula to calculate an angular distribution of the radiated power due to a point dipole placed in a photonic crystal was derived. The formula only involves calculations of the wave vectors, the group velocity, the coupling strength of the dipole moment with the field, and the Gaussian curvature on the isofrequency surface corresponding to the frequency of the oscillating dipole. That can be done by the simple plane-wave expansion method and is not computationally demanding. A numerical example was given for a square-lattice 2D photonic crystal. It was shown by applying the developed formalism and substantiated by FDTD calculations that if a dipole frequency is within a partial photonic band gap, the far-field radiation pattern is strongly modified with respect to the dipole radiation pattern in vacuum, demonstrating suppression in the directions of the spatial stop band and enhancement in the direction of the group velocity, which is stationary with respect to a small variation of the wave vector.

ACKNOWLEDGMENTS

This work was partially supported by EU-IST Project No. APPTech IST-2000-29321 and German BMBF Project No. PCOC 01 BK 253. The author acknowledges A. V. Lavrinenko for making available the FDTD code [65].

[1] E. M. Purcell, Phys. Rev. **69**, 681 (1946).
[2] *Spontaneous Emission and Laser Oscillation in Microcavities*, edited by H. Yokoyama and K. Ujihara (CRC, Boca Raton, 1995).
[3] *Confined Electron and Photon: New Physics and Applications*, edited by E. Burstein and C. Weisbuch (Plenum, New York, 1995).
[4] *Electron Theory and Quantum Electrodynamics: 100 Years Later*, edited by J. P. Dowling (Plenum, New York, 1997).
[5] P. Goy, J. M. Raimond, M. Gross, and S. Haroche, Phys. Rev. Lett. **50**, 1903 (1983).
[6] D. Kleppner, Phys. Rev. Lett. **47**, 233 (1981).
[7] H. Benisty, H. De Neve, and C. Weisbuch, IEEE J. Quantum Electron. **34**, 1612 (1998).
[8] H. Benisty, H. De Neve, and C. Weisbuch, IEEE J. Quantum Electron. **34**, 1632 (1998).
[9] D. Delbeke, R. Bockstaele, P. Bienstman, R. Baets, and H. Benisty, IEEE J. Sel. Top. Quantum Electron. **8**, 189 (2002).
[10] H. Yokoyama and S. D. Brorson, J. Appl. Phys. **66**, 4801 (1989).
[11] G. Bjork, H. Heitmann, and Y. Yamamoto, Phys. Rev. A **47**, 4451 (1993).
[12] G. Bjork, A. Karlsson, and Y. Yamamoto, Phys. Rev. A **50**, 1675 (1994).
[13] J. D. Joannopoulos, R. D. Meade, and J. N. Winn, *Photonic Crystals: Molding the Flow of Light* (Princeton University Press, Princeton, NJ, 1995).
[14] K. Sakoda, *Optical Properties of Photonic Crystals* (Springer, Berlin, 2001).
[15] V. P. Bykov, Sov. Phys. JETP **35**, 269 (1972).
[16] E. Yablonovitch, Phys. Rev. Lett. **58**, 2059 (1987).
[17] S. John and J. Wang, Phys. Rev. Lett. **64**, 2418 (1990).
[18] H. Hirayama, T. Hamano, and Y. Aoyagi, Appl. Phys. Lett. **69**, 791 (1996).
[19] M. Boroditsky, R. Vrijen, T. F Krauss, R. Coccioli, R. Bhat, and E. Yablonovitch, J. Lightwave Technol. **17**, 2096 (1999).
[20] B. Temelkuran, M. Bayindir, E. Ozbay, R. Biswas, M. M. Sigalas, G. Tuttle, and K. M. Ho, J. Appl. Phys. **87**, 603 (2002).
[21] S. Enoch, B. Gralak, and G. Tayeb, Appl. Phys. Lett. **81**, 1588 (2002).
[22] J. P. Dowling and C. M. Bowden, Phys. Rev. A **46**, 612 (1992).
[23] T. Suzuki and P. K. L. Yu, J. Opt. Soc. Am. B **12**, 570 (1995).
[24] K. Sakoda and K. Ohtaka, Phys. Rev. B **54**, 5732 (1996).
[25] Y. Xu, R. K. Lee, and A. Yariv, Phys. Rev. A **61**, 033807 (2000).
[26] V. Lousse, J. P. Vigneron, X. Bouju, and J. M. Vigoureux, Phys. Rev. B **64**, 201104R (2001).
[27] C. Hermann and O. Hess, J. Opt. Soc. Am. B **19**, 3013 (2002).
[28] S. Y. Zhu, Y. Yang, H. Chen, H. Zheng, and M. S. Zubairy, Phys. Rev. Lett. **84**, 2136 (2000).
[29] Z. Y. Li, L. L. Lin, and Z. Q. Zhang, Phys. Rev. Lett. **84**, 4341 (2000).
[30] K. Busch, N. Vats, S. John, and B. C. Sanders, Phys. Rev. E **62**, 4251 (2000).
[31] Z. Y. Li and Y. Xia, Phys. Rev. A **63**, 043817 (2001).
[32] M. Woldeyohannes and S. John, J. Opt. B: Quantum Semiclassical Opt. **5**, R43 (2003).
[33] P. St. J. Russell, Appl. Phys. B: Photophys. Laser Chem. **39**, 231 (1986).
[34] R. Zengerle, J. Mod. Opt. **34**, 1589 (1987).
[35] H. Kosaka, T. Kawashima, A. Tomita, M. Notomi, T. Tamamura, T. Sato, and S. Kawakami, Phys. Rev. B **58**, R10096 (1998).
[36] H. Kosaka, T. Kawashima, A. Tomita, M. Notomi, T. Tamamura, T. Sato, and S. Kawakami, Appl. Phys. Lett. **74**, 1212 (1999).
[37] D. N. Chigrin, S. Enoch, C. M. Sotomayor Torres, and G. Tayeb, Opt. Express **11**, 1203 (2003).

[38] P. Etchegoin and R. T. Phillips, Phys. Rev. B **53**, 12674 (1996).
[39] D. N. Chigrin and C. M. Sotomayor Torres Opt. Spectrosc. **91**, 484 (2001).
[40] J. P. Wolfe, *Imaging Phonons: Acoustic Wave Propagation in Solids* (Cambridge University Press, Cambridge, England, 1998).
[41] B. Taylor, H. J. Maris, and C. Elbaum, Phys. Rev. Lett. **23**, 416 (1969).
[42] G. W. Ford and W. H. Weber, Phys. Rep. **113**, 195 (1984).
[43] R. J. Glauber and M. Lewenstein, Phys. Rev. A **43**, 467 (1991).
[44] G. Allaire, C. Canca, and M. Vanninathan, ESAIM: Proceedings 3, 65 (1998).
[45] J. D. Jackson, *Classical Electrodynamics* (Wiley, New York, 1975).
[46] J. E. Sipe, Surf. Sci. **105**, 489 (1981).
[47] J. M. Wylie and J. E. Sipe, Phys. Rev. A **30**, 1185 (1984).
[48] A. A. Maradudin, in *Phonons and Phonon Interactions*, edited by T. A. Bak (Benjamin, New York, 1964), pp. 424–504.
[49] H. J. Maris, Phys. Rev. B **28**, 7033 (1983).
[50] P. Yeh, *Optical Waves in Layered Media* (Wiley, New York, 1988).
[51] S. V. Gaponenko, V. N. Bogomolov, E. P. Petrov, A. M. Kapitonov, A. A. Eychmueller, A. L. Rogach, I. I. Kalosha, F. Gindele, and U. Woggon, J. Lightwave Technol. **17**, 2128 (1999).
[52] S. G. Romanov, T. Maka, C. M. Sotomayor Torres, M. Muller, and R. Zentel, Appl. Phys. Lett. **79**, 731 (2001).
[53] H. P. Schriemer, H. M. van Driel, A. F. Koenderink, and W. L. Vos, Phys. Rev. A **63**, 011801R (2000).
[54] A. F. Koenderink, L Bechger, H. P. Schriemer, A. Lagendijk, and W. L. Vos, Phys. Rev. Lett. **88**, 143903 (2002).
[55] A. F. Koenderink, L Bechger, A. Lagendijk, and W. L. Vos, Phys. Status Solidi A **197**, 648 (2003).
[56] S. G. Romanov, D. N. Chigrin, V. G. Solovyev, T. Maka, N. Gaponik, A. Eychmuller, A. L. Rogach, and C. M. Sotomayor Torres, Phys. Status Solidi A **197**, 662 (2003).
[57] J. P. Dowling, M. Scalora, M. J. Bloemer, and C. M. Bowden, J. Appl. Phys. **75**, 1896 (1994).
[58] S. Nojima, Jpn. J. Appl. Phys., Part 2 **37**, L565 (1998).
[59] K. Sakoda, Opt. Express **4**, 167 (1999).
[60] G. A. Northrop and J. P. Wolfe, Phys. Rev. B **22**, 6196 (1980).
[61] S. G. Johnson and J. D. Joannopoulos, Opt. Express **8**, 173 (2001).
[62] A. Taflove, *Computational Electrodynamics: The Finite-Difference Time-Domain Method* (Artech House, Norwood, 1995).
[63] D. M. Sullivan, *Electromagnetic Simulation Using the FDTD Method* (IEEE Press, New York, 2002).
[64] J. P. Berenger, J. Comput. Phys. **114**, 185 (1994).
[65] A. Lavrinenko, P. I. Borel, L. H. Frandsen, M. Thorhauge, A. Harpoth, M. Kristensen, T. Niemi, and H. M. H. Chong, Opt. Express **12**, 234 (2004).